Letters

Accurate Modeling of PLL With Frequency-Adaptive Prefilter: On the Positive Feedback Effect

Jiaxing Lei, *Member, IEEE*, Xiangjun Quan, *Member, IEEE*, Shuang Feng, *Member, IEEE*, Jianfeng Zhao, and Wu Chen, *Senior Member, IEEE*

***Abstract*—Phase locked loops (PLLs) with frequency-adaptive prefilters could suppress input disturbances and thus are widely studied. However, their accurate models are absent in the literature. In particular, the impact of frequency adaption (FA) is underestimated. This letter proposes the accurate and analytical modeling method with focus on the impact of frequency adaption, by taking the PLL based on dual second-order generalized integrator (DSOGI) as an example. The proposed model can precisely describe the transient behaviors of DSOGI-PLL, especially the couplings among amplitude, phase angle, and frequency. Moreover, it reveals that the FA creates a positive feedback path, which is the essential reason for the instability phenomenon and the key factor limiting the PLL performance. Experimental results have verified the accuracy of the proposed model.**

***Index Terms*—DSOGI, Frequency adaptive filter, Phase locked loop, Positive feedback effect, Stability.**

I. Introduction

PHASE locked loop (PLL) is a widely used technique for grid synchronization [1]. Since the standard PLL is vulnerable to input unbalance and distortions [2], additional filters are commonly incorporated, such as the moving average filter [3], [4], notch filter [5], delayed signal cancellation operator [6]–[7], dual complex-coefficient filter [8], dual second-order generalized integrator (DSOGI) [9], and others [2]. It is preferable to place the filters before PLL as it does not generate phase delay for the control loop [2]. Besides, parameters of the additional filters are usually frequency adaptive, so as to handle the grid frequency variation in practice. Beneficially, these advanced PLLs could effectively suppress input disturbances at the steady state, even the grid frequency deviates greatly from the nominal value.

It is widely considered that many advanced PLLs are similar or even mathematically equivalent to each other and they have the same small-signal model [2], [10]. This is true for the transfer function from input voltage signal to output signal, if the frequency adaption (FA) is ignored. In [10], additional filters are approximated as an in-loop filter, forming a unified small-signal model. This letter is meaningful as the unified model facilitates tuning of some advanced PLLs. Yet, this unified model is unable to explain the different transient responses of these PLLs. Besides, it cannot accurately describe the couplings among amplitude, phase angle, and frequency. These are mainly because the impact of FA is underestimated, as studied in this letter. It has been found that the stability of SOGI-PLL can be improved if the FA is removed [11]. Similarly, [12] proves that the implementation method of SOGI influences the system stability. Tan *et al.* [13] also show that the implementation method might change the zeros of the transfer functions. Although some discoveries are for the single-phase system, they are applicable to the three-phase system. However, to the best knowledge of authors, there is no analytical and straightforward model provided in literature that can accurately and comprehensively show the impact of FA on three-phase PLLs.

In recent years, it has been extensively demonstrated that the PLL has significant influence on the stability of grid-connected power converters [14]. Therefore, obtaining the accurate model is essential for these advanced PLLs in practical applications. Motivated by this demand, the accurate and analytical small-signal modeling method for these advanced PLLs, with particular focus on the impact of frequency adaption, is proposed by this letter. The DSOGI-PLL is taken as an example since it is superior in many aspects [2], but the proposed method can be easily extended to other advanced PLLs with frequency-adaptive prefilters. The proposed model can accurately describe the transient behaviors of DSOGI-PLL, especially the couplings among amplitude, phase angle, and frequency. Moreover, it reveals that the FA actually yields the positive feedback effect, which is sufficient to explain the stability and performance limits of DSOGI-PLL.

Manuscript received September 15, 2021; revised October 18, 2021; accepted October 30, 2021. Date of publication November 4, 2021; date of current version December 31, 2021. This work was supported in part by the National Natural Science Foundation of China under Grant 52007028, in part by Open Fund Project of State Key Laboratory of HVdc under Grant SKLHVDC-2020-KF-04, and in part by the Zhishan Young Scholar Program of Southeast University, and in part by the National Natural Science Foundation of China under Grant 51477030. *(Corresponding authors: Jiaxing Lei; Shuang Feng.)*

The authors are with the School of Electrical Engineering, Southeast University, Nanjing 210096, China, with the Jiangsu Provincial Key Laboratory of Smart Grid Technology and Equipment, Southeast University, Nanjing 210096, China, and also with Southeast University, Nanjing 210096, China (e-mail: jxlei@seu.edu.cn; xquan@seu.edu.cn; sfeng@seu.edu.cn; jianfeng_zhao@seu.edu.cn; chenwu@seu.edu.cn).

Color versions of one or more figures in this article are available at https://doi.org/10.1109/TPEL.2021.3124930.

Digital Object Identifier 10.1109/TPEL.2021.3124930

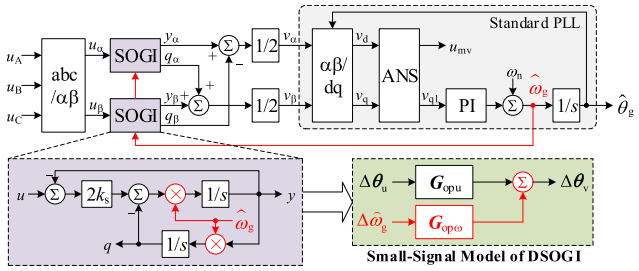

Fig. 1. Schematic diagram of the DSOGI-PLL.

II. Analytical Modeling of DSOGI-PLL

A. Structure of DSOGI-PLL

The schematic diagram of DSOGI-PLL is shown in Fig. 1, where two SOGIs are placed before the standard PLL. With some math operations, the DSOGI acts as the prefilter to suppress the effect of input unbalance. As highlighted in Fig. 1, the grid frequency $\widehat{\omega}_{\mathrm{g}}$ obtained by the standard PLL is fed back to the DSOGI to achieve frequency adaption.

Define $\boldsymbol{u}=u_\alpha+\mathrm{j}u_\beta$ and $\boldsymbol{v}=v_\alpha+\mathrm{j}v_\beta$ as the complex input and output vectors of DSOGI separately. In [10], the scalar transfer functions from $\{u_\alpha,\ u_\beta\}$ to $\{v_\alpha,\ v_\beta\}$ are derived and widely adopted in literature. The equivalent complex form is

$$G_{\mathrm{v}}(s)=\frac{v(s)}{u(s)}=\frac{k_{\mathrm{s}}\widehat{\omega}_{\mathrm{g}}(s+\mathrm{j}\widehat{\omega}_{\mathrm{g}})}{s^2+2k_{\mathrm{s}}\widehat{\omega}_{\mathrm{g}}s+\widehat{\omega}_{\mathrm{g}}^2} \tag{1}$$

where k_{s} is the damping factor of SOGI. Equation (1) is somehow misleading as it implies ignoring the dynamics of $\widehat{\omega}_{\mathrm{g}}$. Yet, it is sufficient to show that $G_{\mathrm{v}}(s)$ has unity gain at the nominal grid frequency ω_{n}, which is true only at the steady state.

B. Novel Small-Signal Model of DSOGI

Generally, a complex vector $\boldsymbol{x}$ can be expressed as

$$x=u_{\mathrm{mx}}e^{\mathrm{j}\theta_{\mathrm{xR}}}=e^{\mathrm{j}(\theta_{\mathrm{xR}}+\mathrm{j}\theta_{\mathrm{xI}})}=e^{\mathrm{j}\theta_{\mathrm{x}}},\quad \theta_{\mathrm{xI}}=-\ln u_{\mathrm{mx}} \tag{2}$$

where u_{mx} is the amplitude and θ_{xR} is the phase angle of $\boldsymbol{x}$. θ_{x} is defined as the complex phase angle of $\boldsymbol{x}$, of which the real part is θ_{xR}, and the imaginary part θ_{xI} is related with u_{mx}. Based on (2), it can be easily obtained that

$$\frac{\mathrm{d}x}{\mathrm{d}t}=\mathrm{j}x\frac{\mathrm{d}\theta_{\mathrm{x}}}{\mathrm{d}t},\quad \frac{\mathrm{d}^2x}{\mathrm{d}t^2}=-x\left(\frac{\mathrm{d}\theta_{\mathrm{x}}}{\mathrm{d}t}\right)^2+\mathrm{j}x\frac{\mathrm{d}^2\theta_{\mathrm{x}}}{\mathrm{d}t^2}. \tag{3}$$

This facilitates the derivation of the proposed model.

According to Fig. 1, DSOGI satisfies the following equations:

$$\begin{cases}\mathrm{d}y_\alpha/\mathrm{d}t=-2k_{\mathrm{s}}\widehat{\omega}_{\mathrm{g}}y_\alpha-\widehat{\omega}_{\mathrm{g}}q_\alpha+2k_{\mathrm{s}}\widehat{\omega}_{\mathrm{g}}u_\alpha\\ \mathrm{d}q_\alpha/\mathrm{d}t=\widehat{\omega}_{\mathrm{g}}y_\alpha\\ \mathrm{d}y_\beta/\mathrm{d}t=-2k_{\mathrm{s}}\widehat{\omega}_{\mathrm{g}}y_\beta-\widehat{\omega}_{\mathrm{g}}q_\beta+2k_{\mathrm{s}}\widehat{\omega}_{\mathrm{g}}u_\beta\\ \mathrm{d}q_\beta/\mathrm{d}t=\widehat{\omega}_{\mathrm{g}}y_\beta\\ v=0.5(y_\alpha-q_\beta)+0.5(y_\beta+q_\alpha)\mathrm{j}.\end{cases} \tag{4}$$

Construct an expression similar to the denominator of (1)

$$\frac{\mathrm{d}^2v}{\mathrm{d}t^2}+2k_{\mathrm{s}}\widehat{\omega}_{\mathrm{g}}\frac{\mathrm{d}v}{\mathrm{d}t}+\widehat{\omega}_{\mathrm{g}}^2v=\left(\frac{\mathrm{d}^2v_\alpha}{\mathrm{d}t^2}+2k_{\mathrm{s}}\widehat{\omega}_{\mathrm{g}}\frac{\mathrm{d}v_\alpha}{\mathrm{d}t}+\widehat{\omega}_{\mathrm{g}}^2v_\alpha\right)+\mathrm{j}\left(\frac{\mathrm{d}^2v_\beta}{\mathrm{d}t^2}+2k_{\mathrm{s}}\widehat{\omega}_{\mathrm{g}}\frac{\mathrm{d}v_\beta}{\mathrm{d}t}+\widehat{\omega}_{\mathrm{g}}^2v_\beta\right). \tag{5}$$

With the substitution of (4), (5) turns to

$$\frac{\mathrm{d}^2v}{\mathrm{d}t^2}+2k_{\mathrm{s}}\widehat{\omega}_{\mathrm{g}}\frac{\mathrm{d}v}{\mathrm{d}t}+\widehat{\omega}_{\mathrm{g}}^2v=k_{\mathrm{s}}\widehat{\omega}_{\mathrm{g}}\left(\frac{\mathrm{d}u}{\mathrm{d}t}+\mathrm{j}\widehat{\omega}_{\mathrm{g}}u\right)+(\mathrm{j}v-2k_{\mathrm{s}}e_{\mathrm{y}})\frac{\mathrm{d}\widehat{\omega}_{\mathrm{g}}}{\mathrm{d}t} \tag{6}$$

where $\boldsymbol{e}_{\mathrm{y}}$ is defined as $\boldsymbol{y}$-$\boldsymbol{u}$. The deduction of (6) is tedious but quite straightforward. Like other parts containing $\widehat{\omega}_{\mathrm{g}}$, the part highlighted by red in (6) also contributes to the impact of $\widehat{\omega}_{\mathrm{g}}$ on the dynamics of $\boldsymbol{v}$. If one directly derives the differential equation from (1), this important part will be lost, resulting in an inaccurate model. This is why (1) is misleading.

According to (3), (6) is rewritten as

$$-v\left(\frac{\mathrm{d}\theta_{\mathrm{v}}}{\mathrm{d}t}\right)^2+\mathrm{j}v\frac{\mathrm{d}^2\theta_{\mathrm{v}}}{\mathrm{d}t^2}+2\mathrm{j}k_{\mathrm{s}}\widehat{\omega}_{\mathrm{g}}v\frac{\mathrm{d}\theta_{\mathrm{v}}}{\mathrm{d}t}+\widehat{\omega}_{\mathrm{g}}^2v=k_{\mathrm{s}}\widehat{\omega}_{\mathrm{g}}\left(\mathrm{j}u\frac{\mathrm{d}\theta_{\mathrm{u}}}{\mathrm{d}t}+\mathrm{j}\widehat{\omega}_{\mathrm{g}}u\right)+(\mathrm{j}v-2k_{\mathrm{s}}e_{\mathrm{y}})\frac{\mathrm{d}\widehat{\omega}_{\mathrm{g}}}{\mathrm{d}t}. \tag{7}$$

By multiplying a vector $v_1=e^{-\mathrm{j}\theta_{\mathrm{v}}}$ at both sides of the equal sign, (7) is simplified as

$$-\left(\frac{\mathrm{d}\theta_{\mathrm{v}}}{\mathrm{d}t}\right)^2+\mathrm{j}\frac{\mathrm{d}^2\theta_{\mathrm{v}}}{\mathrm{d}t^2}+2\mathrm{j}k_{\mathrm{s}}\widehat{\omega}_{\mathrm{g}}\frac{\mathrm{d}\theta_{\mathrm{v}}}{\mathrm{d}t}+\widehat{\omega}_{\mathrm{g}}^2=k_{\mathrm{s}}\widehat{\omega}_{\mathrm{g}}\left(\mathrm{j}\frac{\mathrm{d}\theta_{\mathrm{u}}}{\mathrm{d}t}+\mathrm{j}\widehat{\omega}_{\mathrm{g}}\right)e^{\mathrm{j}(\theta_{\mathrm{u}}-\theta_{\mathrm{v}})}+(\mathrm{j}-2k_{\mathrm{s}}e_{\mathrm{y}}v_1)\frac{\mathrm{d}\widehat{\omega}_{\mathrm{g}}}{\mathrm{d}t}. \tag{8}$$

Note that $\boldsymbol{e}_{\mathrm{y}}$ is zero at the steady state since the SOGI has unity gain from $\boldsymbol{u}$ to $\boldsymbol{y}$ at the nominal grid frequency.

Considering the small-signal variations, θ_{v}, θ_{u}, and $\widehat{\omega}_{\mathrm{g}}$ can be expressed as

$$\theta_{\mathrm{v}}=\omega_{\mathrm{n}}t+\Delta\theta_{\mathrm{v}},\quad \theta_{\mathrm{u}}=\omega_{\mathrm{n}}t+\Delta\theta_{\mathrm{u}},\quad \widehat{\omega}_{\mathrm{g}}=\omega_{\mathrm{n}}+\Delta\widehat{\omega}_{\mathrm{g}}. \tag{9}$$

By substituting (9) into (8) with some math manipulations, one can obtain

$$\mathrm{j}\frac{\mathrm{d}^2\Delta\theta_{\mathrm{v}}}{\mathrm{d}t^2}+2\omega_{\mathrm{n}}(\mathrm{j}k_{\mathrm{s}}-1)\frac{\mathrm{d}\Delta\theta_{\mathrm{v}}}{\mathrm{d}t}-2k_{\mathrm{s}}\omega_{\mathrm{n}}^2\Delta\theta_{\mathrm{v}}=\mathrm{j}k_{\mathrm{s}}\omega_{\mathrm{n}}\frac{\mathrm{d}\Delta\theta_{\mathrm{u}}}{\mathrm{d}t}-2k_{\mathrm{s}}\omega_{\mathrm{n}}^2\Delta\theta_{\mathrm{u}}+\mathrm{j}\frac{\mathrm{d}\widehat{\omega}_{\mathrm{g}}}{\mathrm{d}t}+(\mathrm{j}k_{\mathrm{s}}-2)\omega_{\mathrm{n}}\Delta\widehat{\omega}_{\mathrm{g}}. \tag{10}$$

By separating the real and imaginary parts and transforming to the s-domain, (10) results in

$$\begin{bmatrix}\Delta\theta_{\mathrm{vR}}(s)\\ \Delta\theta_{\mathrm{vI}}(s)\end{bmatrix}=A^{-1}B\begin{bmatrix}\Delta\theta_{\mathrm{uR}}(s)\\ \Delta\theta_{\mathrm{uI}}(s)\end{bmatrix}+A^{-1}C\Delta\widehat{\omega}_{\mathrm{g}}(s)=G_{\mathrm{opu}}\begin{bmatrix}\Delta\theta_{\mathrm{uR}}(s)\\ \Delta\theta_{\mathrm{uI}}(s)\end{bmatrix}+G_{\mathrm{op}\omega}\Delta\widehat{\omega}_{\mathrm{g}}(s) \tag{11}$$

where matrices $\boldsymbol{A}$, $\boldsymbol{B}$, and $\boldsymbol{C}$ are expressed as

$$\begin{cases} A = \begin{bmatrix} 2\omega_{\mathrm{n}}s + 2k_{\mathrm{s}}\omega_{\mathrm{n}}^2 & s^2 + 2k_{\mathrm{s}}\omega_{\mathrm{n}}s \\ s^2 + 2k_{\mathrm{s}}\omega_{\mathrm{n}}s & -2\omega_{\mathrm{n}}s - 2k_{\mathrm{s}}\omega_{\mathrm{n}}^2 \end{bmatrix} \\ B = \begin{bmatrix} 2k_{\mathrm{s}}\omega_{\mathrm{n}}^2 & k_{\mathrm{s}}\omega_{\mathrm{n}}s \\ k_{\mathrm{s}}\omega_{\mathrm{n}}s & -2k_{\mathrm{s}}\omega_{\mathrm{n}}^2 \end{bmatrix}, \; C = \begin{bmatrix} 2\omega_{\mathrm{n}} \\ s + k_{\mathrm{s}}\omega_{\mathrm{n}} \end{bmatrix}. \end{cases} \tag{12}$$

Matrices $\boldsymbol{G}_{\mathrm{opu}}$ and $\boldsymbol{G}_{\mathrm{op}\omega}$ represent the open-loop transfer functions from $\Delta\theta_{\mathrm{u}}$and $\Delta\widehat{\omega}_{\mathrm{g}}$ to $\Delta\theta_{\mathrm{v}}$, respectively.

Equation (11) denotes the accurate small-signal model of DSOGI, which is illustrated in Fig. 1. Some other prefilters used to be considered equivalent with DSOGI because they do have the same matrices $\boldsymbol{A}$ and $\boldsymbol{B}$ with (12). However, the matrix $\boldsymbol{C}$ would be quite different since the differential aligns shown in (4) highly depends on the implementation of prefilters. As analyzed in the next, the matrix $\boldsymbol{C}$ has significant influence on the dynamic performance of these PLLs. Nevertheless, the last part of (11) has gained rare attentions to date.

C. Closed-Loop Model of DSOGI-PLL

For the standard PLL, the transfer function of the phase angle loop is expressed as $G_{\mathrm{PLL}}(s)$ [2]

$$G_{\mathrm{PLL}}(s) = \frac{\Delta\widehat{\theta}_{\mathrm{g}}(s)}{\Delta\theta_{\mathrm{vR}}(s)} = \frac{k_{\mathrm{p}}s + k_{\mathrm{i}}}{s^2 + k_{\mathrm{p}}s + k_{\mathrm{i}}} \tag{13}$$

where k_{p} and k_{i} are the parameters of the proportional–integral (PI) controller in the PLL, which can be expressed as

$$k_{\mathrm{p}} = 2\xi_{\mathrm{PLL}}\omega_{\mathrm{PLL}}, \; k_{\mathrm{i}} = \omega_{\mathrm{PLL}}^2 \tag{14}$$

where ξ_{PLL} and ω_{PLL} denote the damping factor and natural frequency of PLL separately. Note the amplitude normalization scheme should be applied to decouple the amplitude and phase angle at the PLL stage. According to Fig. 1, the small-signal variation of the detected frequency $\widehat{\omega}_{\mathrm{g}}$ satisfies

$$\Delta\widehat{\omega}_{\mathrm{g}}(s) = s\Delta\widehat{\theta}_{\mathrm{g}}(s). \tag{15}$$

By combining (11), (13), and (15) with some math operation, the closed-loop model of DSOGI-PLL is obtained

$$\begin{bmatrix} \Delta\widehat{\theta}_{\mathrm{g}}(s) \\ \Delta\theta_{\mathrm{vI}}(s) \end{bmatrix} = G_{\mathrm{cl}}(s) \begin{bmatrix} \Delta\theta_{\mathrm{uR}}(s) \\ \Delta\theta_{\mathrm{uI}}(s) \end{bmatrix} \tag{16}$$

where the closed-loop transfer function $\boldsymbol{G}_{\mathrm{cl}}(s)$ is expressed as

$$G_{\mathrm{cl}}(s) = \begin{bmatrix} G_{\mathrm{PLL}} & 0 \\ 0 & 1 \end{bmatrix} \left(I - G_{\mathrm{op}\omega} \cdot \begin{bmatrix} sG_{\mathrm{PLL}} & 0 \end{bmatrix}\right)^{-1} G_{\mathrm{opu}}. \tag{17}$$

It can be seen that, by defining the complex phase angle, the obtained (17) is relatively concise and confine. Yet, the actual amplitude is more commonly used in practice. According to (2), imaginary parts of the complex phase angles are associated with the small-signal variations of amplitudes

$$\begin{cases} \Delta\theta_{\mathrm{vI}} = \left.\frac{\mathrm{d}(-\ln u_{\mathrm{mv}})}{\mathrm{d}u_{\mathrm{mv}}}\right|_{u_{\mathrm{mv}}=U_{\mathrm{mv0}}} \cdot \Delta u_{\mathrm{mv}} = -\frac{\Delta u_{\mathrm{mv}}}{U_{\mathrm{mv0}}} \\ \Delta\theta_{\mathrm{uI}} = \left.\frac{\mathrm{d}(-\ln u_{\mathrm{mu}})}{\mathrm{d}u_{\mathrm{mu}}}\right|_{u_{\mathrm{mu}}=U_{\mathrm{mu0}}} \cdot \Delta u_{\mathrm{mu}} = -\frac{\Delta u_{\mathrm{mu}}}{U_{\mathrm{mu0}}} \end{cases} \tag{18}$$

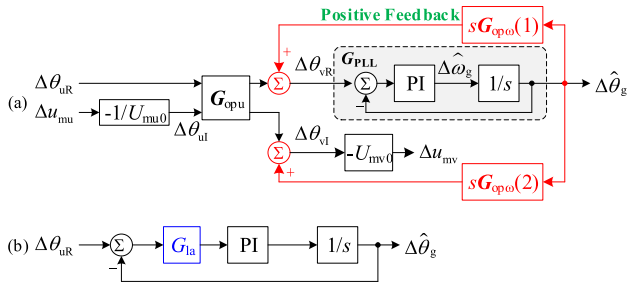

Fig. 2. Small-signal models of DSOGI-PLL. (a) Proposed model. (b) Conventional unified model [10].

where U_{mv0} and U_{mu0} represent the steady-state amplitudes. Based on (17) and (18), the proposed small-signal model of DSOGI-PLL is illustrated in Fig. 2(a).

Equation (16) is an analytical model accurately describing the transient behaviors of the DSOGI-PLL. Beneficially, the coupling effect, which is the intrinsic dynamic feature of DSOGI-PLL, is intuitive from Fig. 2(a). The coupling is mainly reflected by that $\boldsymbol{G}_{\mathrm{opu}}$ is not a diagonal matrix as shown in (11) and (12). When the amplitude or the phase angle of input voltages is disturbed, both the amplitude and phase angle of the output signal of DSOGI will be affected simultaneously. It can be known from the deduction process that the coupling is introduced by DSOGI which acts as the prefilter. Two SOGIs are implemented on the α-axis and β-axis signals separately, rather than the amplitude and phase angle. Consequently, the DSOGI always influences the amplitude and phase angle simultaneously. As to the coupling associated with frequency, it is because the frequency is always the derivative of the phase angle, as shown in (15). Any disturbance in the frequency corresponds to a variation in the phase angle, and vice versa. Note that the coupling phenomena have been widely acknowledged in the literature [10]. Yet, the proposed model can accurately and quantitatively analyze the coupling effect of DSOGI-PLL.

The conventional unified small-signal model proposed in [10] is illustrated in Fig. 2(b). This model is only suitable for the phase angle or the frequency. The function of prefilters is approximated by a transfer function $G_{\mathrm{la}}(s)$ located in the loop of PLL. It is clear that this model is different from the proposed model. By comparing the deduction processes presented in [10] and this letter, it can be known that the unified model in [10] does not pay full attention to the impact of frequency adaption. Besides, the accurate model for analyzing the coupling effect is not provided in [10].

D. Positive Feedback Effect

The control paths highlighted by red in Fig. 2(a) represent the impact of the frequency adaption. It is clear that the upper path forms an additional closed-loop while the lower path does not. Therefore, the upper path could influence the system stability but the lower path could not, which can also be known from (17). Actually, the upper path yields positive feedback control, which has not been revealed before. Due to the positive feedback effect, the DSOGI-PLL with improper parameters could easily

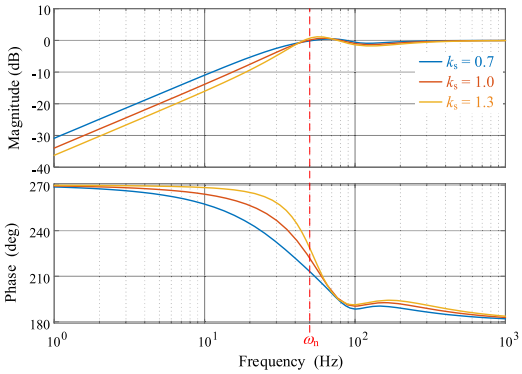

Fig. 3. Frequency responses of $-sG_{op\omega}(1)$ with different k_s.

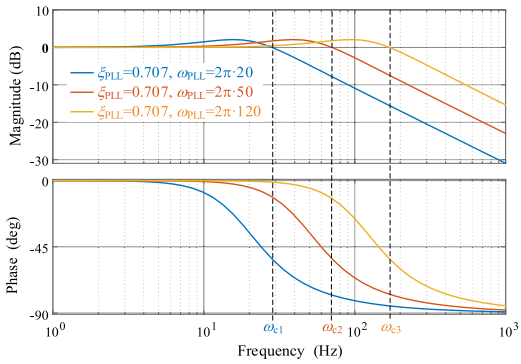

Fig. 4. Frequency responses of G_{PLL} with different k_p and k_i, $k_p = 2\xi_{PLL}\omega_{PLL}$, and $k_i = \omega_{PLL}{}^2$.

become unstable. Therefore, the PLL must be tuned to ensure that $-s\boldsymbol{G}_{op\omega}(1)\cdot G_{PLL}$ has sufficient gain margin and phase margin. This also means that the DSOGI and PLL cannot be tuned separately if the FA is applied.

To further explain this effect, frequency responses of $-s\boldsymbol{G}_{op\omega}(1)$ and G_{PLL} with different parameters are shown in Figs. 3 and 4, respectively. It is clear that the magnitude of $-s\boldsymbol{G}_{op\omega}(1)$ approaches unity and the phase angle approaches 180°, when the frequency is higher than ω_n. This means that $-s\boldsymbol{G}_{op\omega}(1)$ itself is approximately critically stable. For G_{PLL}, the magnitude is always larger than unity in the frequency range slightly lower than the crossing frequency ω_c. Besides, G_{PLL} is a low-pass filter which generates obvious phase delay (≥45° in Fig. 4) at ω_c. Therefore, ω_c of G_{PLL} must be sufficiently low, otherwise $-s\boldsymbol{G}_{op\omega}(1)\cdot G_{PLL}$ will have negative gain margin or phase margin, leading to the unstable DSOGI-PLL.

The crossing frequency ω_c of PLL satisfies $|G_{PLL}(j\omega_c)| = 1$. According to (13) and (14), ω_c can be expressed as

$$\omega_c = \sqrt{2}\omega_{PLL}. \tag{19}$$

With the analytical transfer function shown in (17), the exact crossing frequency ω_c of PLL at the stability boundary can be obtained with different values of k_s and ξ_{PLL}, which is illustrated in Fig. 5. It shows that ω_c at the stability boundary is mostly lower than ω_n. Moreover, ω_c should be even much lower (e.g., 50%) than its critical value in practice, so as to

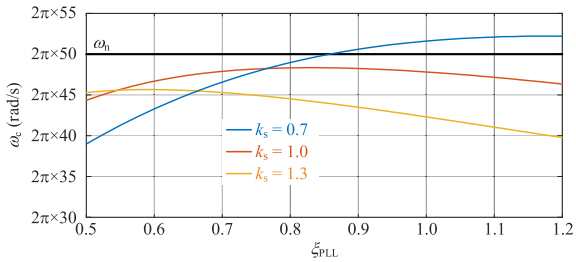

Fig. 5. Crossing frequency ω_c of G_{PLL} at the stability boundary.

ensure sufficient stability margin. This is why the FA limits the dynamic performance of DSOGI-PLL.

Being stable is only the minimum requirement. The fast and smooth dynamic performance of DSOGI-PLL is more desirable in practice, which is collectively decided by k_s, ξ_{PLL} and ω_{PLL}. Theoretically, the accurate and analytical model provided in (17) can be used to obtain the optimal values of k_s, ξ_{PLL}, and ω_{PLL}. However, interested readers will find that, because the performance of DSOGI-PLL is highly limited by the frequency adaption, the applicable values are in very narrow ranges and the optimal performance is quite close to that obtained by [10]. Therefore, the optimization is not presented in this letter due to the limited space. Performance of other PLL structures can also be analyzed with the similar method, whereas the quantitative conclusion could be different.

Moreover, Fig. 2(a) is able to explain the effect of fixed frequency operation. In this case, the control paths highlighted by red are broken, and $\boldsymbol{G}_{cl}(s)$ becomes

$$G_{cl}(s) = \begin{bmatrix} G_{PLL} & 0 \\ 0 & 1 \end{bmatrix} G_{opu}. \tag{20}$$

Based on the expressions of $\boldsymbol{G}_{opu}$ and G_{PLL}, it can be known that they are always stable with positive k_s, k_p, and k_i, which is why the fixed-frequency operation could improve the stability. In this case, parameters of DSOGI and PLL can be tuned separately to achieve smooth and fast dynamic responses. Yet, it is at the cost of lower disturbance rejection capability under deviated grid frequency.

III. Experimental Verification

To verify the accuracy of the proposed small-signal model, the DSOGI-PLL in Fig. 1 is implemented in a digital signal processor. Note that the performance of DSOGI-PLL is sensitive to the implementation of DSOGI. Therefore, the experimental code should strictly comply with the structure shown in Fig. 1. Unless otherwise stated, parameters of the DSOGI-PLL provided by [10] are adopted in the experiments: $k_s = 1.056$, $\xi_{PLL} = 0.7746$, and $\omega_{PLL} = 2\pi\times14.20$ rad/s.

First, the validation is realized in the frequency domain. The results are shown in Fig. 6. The theoretical frequency responses of the proposed model are obtained based on (17), whereas the actual responses are obtained by injecting signals at the amplitude or phase angle of input voltages. Frequencies of the injected signals spread logarithmically in the range of 1∼1000 Hz. The theoretical frequency response of the conventional model is

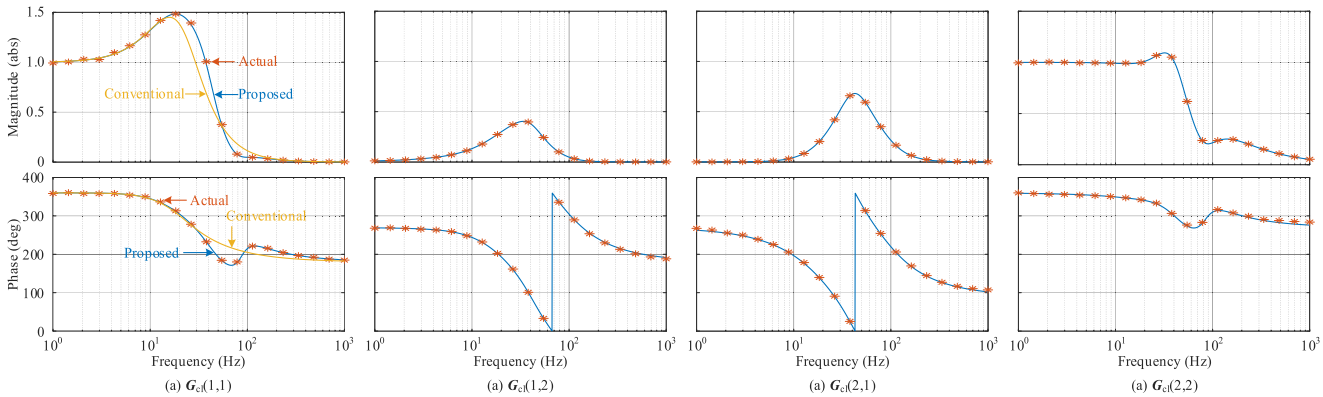

Fig. 6. Model validation in the frequency domain: the blue and solid lines denote the theoretical frequency responses obtained with (17); the stars denote the actual responses obtained by injecting harmonics in experiments; the yellow lines denote the responses of conventional model. Note that only the transfer function corresponding to $\boldsymbol{G}_{cl}(1,1)$ is available in the literature.

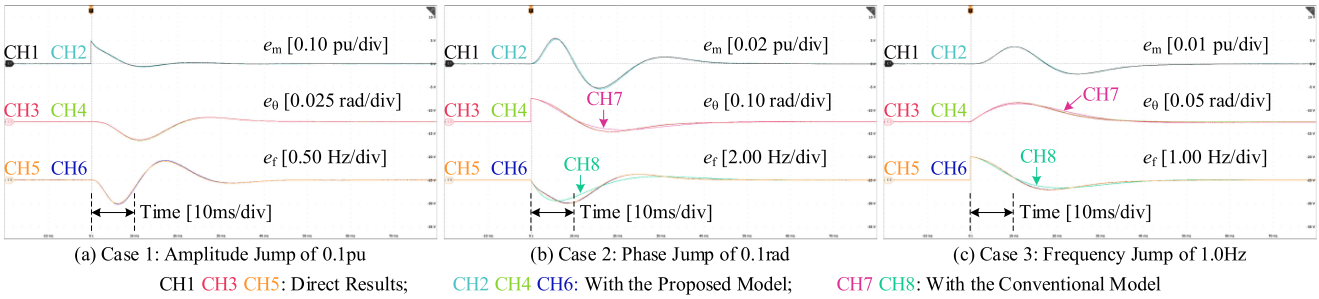

(a) Case 1: Amplitude Jump of 0.1pu (b) Case 2: Phase Jump of 0.1rad (c) Case 3: Frequency Jump of 1.0Hz

CH1 CH3 CH5: Direct Results; CH2 CH4 CH6: With the Proposed Model; CH7 CH8: With the Conventional Model

Fig. 7. Experimental results with amplitude, phase angle, and frequency jumps. Results with the proposed model are almost overlapped with the direct results.

TABLE I
ACCURACY OF THE SMALL-SIGNAL MODELS

Case No.	Proposed			Conventional		
	Amp.	Phase	Freq.	Amp.	Phase	Freq.
1	2.4×10^{-3}	9.4×10^{-4}	3.2×10^{-2}	---	---	---
2	1.8×10^{-3}	2.2×10^{-3}	6.6×10^{-2}	---	1.2×10^{-2}	4.6×10^{-1}
3	4.8×10^{-4}	1.1×10^{-3}	1.7×10^{-2}	---	4.5×10^{-3}	1.3×10^{-1}

also presented in Fig. 6(a). Note that only the transfer function corresponding to $\boldsymbol{G}_{cl}(1,1)$ is available in the literature. It is clear that the proposed model has almost the same frequency responses with the actual responses in a wide frequency range, proving the high accuracy of the proposed model in frequency domain. On the contrary, the conventional model is inaccurate in the medium frequency range.

Second, the validation is realized in the time domain. Three cases with jumps of amplitude, phase angle and frequency are presented in Fig. 7, where all variables represent the errors between the input signal and the response in time domain. The direct results are obtained with the DSOG-PLL shown in Fig. 1, while the model results are obtained with the transfer function shown in (17). It can be seen that, in all cases, waveforms obtained with the proposed small-signal model are almost overlapped with the direct experimental results, indicating the high accuracy. On the contrary, obvious differences can be observed with the conventional model. Table I lists the quantitative results, where the accuracy is defined as the maximum difference between the direct experimental results and the small-signal models. It is clear that the accuracy of the proposed model is improved at least 4 times and up to 10 times. In particular, the accuracy of the proposed model describing the couplings among amplitude, phase angle, and frequency are also very high, whereas the accurate coupling model is unavailable from literature. This also proves one advantage of the proposed model in practical applications, where the common grounding faults could cause severe disturbances on the amplitude and/or phase angle of grid voltages. The proposed model can thus be used to evaluate the transient performance of DSOGI-PLL after grid faults.

Third, the experimental results with FA initially disabled and then enabled are illustrated in Fig. 8. In this case, k_s and ξ_{PLL} remain 1.056 and 0.7746, respectively. With the provided analytical model, it can be calculated that the crossing frequency ω_c of PLL at the stability boundary is about $2\pi\times47.73$ rad/s. Accordingly, the critical ω_{PLL} is $2\pi\times33.75$ rad/s, which is applied to the PLL in this case. Both the DSOGI and PLL could achieve fast and smooth transient responses if they work separately. Phase jumps are applied to test the dynamic responses. Fig. 8 shows that, without the frequency adaption, the DSOGI-PLL is stable with a superior dynamic response. However, when the FA is enabled, unattenuated oscillations occur on all the waveforms. This proves the FA reduces the stability of DSOGI-PLL. Noticeably, the proposed small-signal model coincides well with the direct experimental results in the whole process, demonstrating the high accuracy of the proposed model.

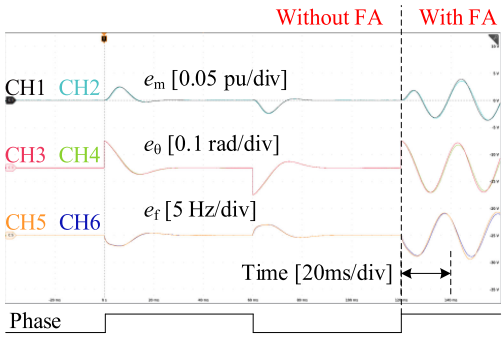

Fig. 8. Experimental results with and without FA.

IV. Conclusion

Aimed at the advanced PLL with a prefilter, this letter has proven that the FA actually creates a positive feedback control path. Ignoring such an effect could result in low accuracy of the small-signal model. The positive feedback control also accounts for the instability phenomenon associated with the frequency adaption. Based on the proposed modeling method, it can be inferred that the advanced PLLs which were considered equivalent to each other actually have noticeable differences in the transients, since their implementations of the FA are quite different. Besides, the proposed model also benefits the improvement of PLL performance, from both parameters and structures.

References

[1] S. Golestan, J. M. Guerrero, J. C. Vasquez, A. M. Abusorrah, and Y. Al-Turki, "Linear time-periodic modeling, examination, and performance enhancement of grid synchronization systems with DC component rejection/estimation capability," *IEEE Trans. Power Electron.*, vol. 36, no. 4, pp. 4237–4253, Apr. 2021.

[2] S. Golestan, J. M. Guerrero, and J. C. Vasquez, "Three-Phase PLLs: A review of recent advances," *IEEE Trans. Power Electron.*, vol. 32, no. 3, pp. 1894–1907, Mar. 2017.

[3] S. Golestan, M. Ramezani, J. M. Guerrero, F. D. Freijedo, and M. Monfared, "Moving average filter based phase-locked loops: Performance analysis and design guidelines," *IEEE Trans. Power Electron.*, vol. 29, no. 6, pp. 2750–2763, Jun. 2014.

[4] A. K. Verma, R. K. Jarial, M. R. Ungarala, and P. Roncero-Sanchez, "A robust three-phase pre-filtered phase locked-loop for the sub-cycle estimation of fundamental parameters," *IEEE Trans. Ind. Appl.*, to be published, doi: 10.1109/TIA.2021.3105615.

[5] F. Gonzalez-Espin, E. Figueres, and G. Garcera, "An adaptive synchronous-reference-frame phase-locked loop for power quality improvement in a polluted utility grid," *IEEE Trans. Ind. Electron.*, vol. 59, no. 6, pp. 2718–2731, Jun. 2012.

[6] M. Rasheduzzaman and J. W. Kimball, "Modeling and tuning of an improved delayed-signal-cancellation PLL for microgrid application," *IEEE Trans. Energy Convers.*, vol. 34, no. 2, pp. 712–721, Jun. 2019.

[7] M. S. Reza, F. Sadeque, M. M. Hossain, A. M. Y. M. Ghias, and V. G. Agelidis, "Three-phase PLL for grid-connected power converters under both amplitude and phase unbalanced conditions," *IEEE Trans. Ind. Electron.*, vol. 66, no. 11, pp. 8881–8891, Nov. 2019.

[8] M. Ramezani, S. Golestan, S. Li, and J. M. Guerrero, "A simple approach to enhance the performance of complex-coefficient filter-based PLL in grid-connected applications," *IEEE Trans. Ind. Electron.*, vol. 65, no. 6, pp. 5081–5085, Jun. 2018.

[9] A. A. Nazib, D. G. Holmes, and B. P. McGrath, "Decoupled DSOGI-PLL for improved three phase grid synchronisation," in *Proc. Int. Power Electron. Conf.*, Niigata, Japan, 2018, pp. 3670–3677.

[10] S. Golestan, M. Monfared, and F. D. Freijedo, "Design-oriented study of advanced synchronous reference frame phase-locked loops," *IEEE Trans. Power Electron.*, vol. 38, no. 2, pp. 765–778, Feb. 2013.

[11] F. Xiao, L. Dong, L. Li, and X. Liao, "A frequency-fixed SOGI-based PLL for single-phase grid-connected converters," *IEEE Trans. Power Electron.*, vol. 32, no. 3, pp. 1713–1719, Mar. 2017.

[12] C. Zhang, S. Føyen, J. A. Suul, and M. Molinas, "Modeling and analysis of SOGI-PLL/FLL-based synchronization units: Stability impacts of different frequency-feedback paths," *IEEE Trans. Energy Convers.*, vol. 36, no. 3, pp. 2047–2058, Sep. 2021.

[13] G. Tan, X. Zeng, Y. Zhang, J. Wei, Z. Chen, and X. Sun, "Model linearization analysis for three-phase unbalanced phase-locked loop techniques," in *Proc. IEEE 4th Int. Elect. Energy Conf.*, Wuhan, China, 2021, pp. 1–6.

[14] H. Wu and X. Wang, "Design-oriented transient stability analysis of PLL-synchronized voltage-source converters," *IEEE Trans. Power Electron.*, vol. 35, no. 4, pp. 3573–3589, Apr. 2020.